Hydrol. Earth Syst. Sci. Discuss., https://doi.org/10.5194/hess-2019-95
Manuscript under review for journal Hydrol. Earth Syst. Sci.
Discussion started: 22 March 2019


Hydrology and Earth System Sciences
Open Access
Discussions

# Assessment of Simulated Soil Moisture from WRF Noah, Noah-MP, and CLM Land Surface Schemes for Landslide Hazard Application

Lu Zhuo[1], Qiang Dai[1,2*], Dawei Han[1], Ningsheng Chen[3], Binru Zhao[1,4]

[1]WEMRC, Department of Civil Engineering, University of Bristol, Bristol, UK

[2]Key Laboratory of VGE of Ministry of Education, Nanjing Normal University, Nanjing, China

[3]The Institute of Mountain Hazards and Environment (IMHE), China

[4]College of Water Conservancy and Hydropower Engineering, Hohai University, Nanjing, China

[*]Correspondence: civengwater@gmail.com

## Abstract

This study assesses the usability of Weather Research and Forecasting (WRF) model simulated soil moisture for landslide monitoring in the Emilia Romagna region, northern Italy during the 10-year period between 2006 and 2015. Particularly three advanced Land Surface Model (LSM) schemes (i.e., Noah, Noah-MP and CLM4) integrated with the WRF are used to provide comprehensive multi-layer soil moisture information. Through the temporal evaluation with the in-situ soil moisture observations, Noah-MP is the only scheme that is able to simulate the large soil drying phenomenon close to the observations during the dry season, and it also has the highest correlation coefficient and the lowest *RMSE* at most soil layers. Each simulated soil moisture product from the three LSM schemes is then used to build a landslide threshold model, and within each model, 17 different exceedance probably levels from 1% to 50% are adopted to determine the optimal threshold scenario (in total there are 612 scenarios). Slope degree information is also used to separate the study region into different groups. The threshold evaluation performance is based on the landslide forecasting accuracy using 45 selected rainfall events between 2014-2015. Contingency tables, statistical indicators, and Receiver Operating Characteristic analysis for different threshold scenarios are explored. The results have shown that the slope information is very useful in identifying threshold differences, with the threshold becoming smaller for the steeper area. For landslide monitoring, Noah-MP at the surface soil layer with 30% exceedance probability provides the best landslide monitoring performance, with its hitting rate at 0.769, and its false alarm rate at 0.289.

**Keywords:** Emilia Romagna, Weather Research and Forecasting (WRF) Model, Land Surface Model (LSM), Numerical Weather Prediction (NWP) model, landslide hazards, soil moisture.

## 1. Introduction

Landslide is a repeated geological hazard during rainfall seasons, which causes massive destructions, loss of lives, and economic damages worldwide (Klose et al., 2014). It is estimated between 2004 and 2016, there is a total number of 4862 fatal non-seismic landslides occurred around the world, which had resulted in the death of over 55,000 people (Froude and Petley, 2018). Those numbers are expected to further increase due to extreme events induced by climate changes and pressures of population expanding towards unstable hillside areas (Gariano and Guzzetti, 2016;Petley, 2012). The accurate predicting and monitoring of the spatiotemporal occurrence of the landslide is the key to prevent/ reduce casualties and damages to properties and infrastructures. The most widely adopted method for real-time landslide monitoring is based on the simple empirical rainfall threshold, which has been used in many countries for their national landslide early warning system (Caine, 1980). The method commonly relies on building the rainfall intensity-duration curve using the information from the past landslide events (Chae et al., 2017). However, such a method in many cases is insufficient for landslide hazard assessment (Posner and Georgakakos, 2015), because in addition to rainfall, initial soil moisture condition is one of the main triggering factors of the events (Glade et al., 2000;Crozier, 1999;Tsai and Chen, 2010;Hawke and McConchie, 2011;Bittelli et al., 2012;Segoni et al., 2018;Valenzuela et al., 2018;Bogaard and Greco, 2018).

Although some researches have recognised the significance of soil moisture information for landslide early warning, most of them only rely on the antecedent precipitation index which simply depends on the amount of total rainfall accumulated before a landslide event occurs (Chleborad, 2003;Calvello et al., 2015;Zêzere et al., 2005). Such a method is not recommended by several studies (Pelletier et al., 1997;Baum and Godt, 2010;Brocca et al., 2008), because during wet seasons, soil is often already saturated, and any additional rainfall falls on the earth surface will become direct runoff (Zhuo and Han, 2016b, a). As a result, the antecedent precipitation method can sometimes significantly overestimate the soil wetness condition. On the other hand, evapotranspiration is another factor which controls the soil moisture temporal evolution, which can also influence the relationship between the actual and the estimated soil moisture. Therefore, it is important that the landslide hazard assessment should be based on the real soil moisture information.

Soil moisture varies largely both spatially and temporally (Zhuo et al., 2015b). For landslide applications, to accurately monitor soil moisture fluctuations in a critical zone (normally in remote regions), a dense network of soil moisture sensors is prerequisite. However, because of the complex installation and high maintenance fee especially in steep mountainous areas, such networks are normally unavailable. Several studies have found the usefulness of ground-measured soil moisture data for landslide monitoring purpose (Greco et al., 2010;Baum and Godt, 2010;Harris et al., 2012;Hawke and McConchie, 2011). However, due to the sparse distribution/no existence of in-situ sensors in most hazardous regions, alternative soil moisture data sources need to be explored. One of the data sources is through satellite remote sensing technologies. Although such technologies have been improved significantly over the past decade (Zhuo et al., 2016a), their retrieving accuracy is still largely affected by meteorological conditions (cloud coverage and rainfall), frozen soil conditions (Zhuo et al., 2015a), and dense vegetation coverages particularly in mountainous regions (Temimi et al., 2010); furthermore, the acquired data only covers the top few centimetres of soil, and their resolution is too low (e.g., 0.25 degree) for detailed regional studies (Zhuo et al., 2016b). Those disadvantages restrict the full utilisation of satellite soil moisture products for landslide monitoring application as discussed in Zhuo et al. (2019).

Another soil moisture data source relies on the state-of-the-art Land Surface Models (LSMs) such as the Noah LSM (Ek et al., 2003) and the Community Land Model (CLM) (Oleson et al., 2010). LSMs describe the interactions between the atmosphere and the land surface by simulating exchanges of momentum, heat and water within the Earth system (Maheu et al., 2018). They are capable of simulating the most important subsurface hydrological processes (e.g., soil moisture) and can be integrated with the advanced Numerical Weather Prediction (NWP) system like WRF (Weather Research and Forecasting) (Skamarock et al., 2008) for comprehensive soil moisture estimations (i.e., through the surface energy balance, the surface layer stability and the water balance equations) (Greve et al., 2013). NWP-based (i.e., with integrated LSM, thereafter) soil moisture estimations have many advantages, for instance their spatial and temporal resolution can be set discretionarily to fit different application requirements; their coverage is global, and the estimated soil moisture data covers multiple soil layers (from the shallow surface layer to deep root-zones); as well as a number of globally-covered data products can provide the necessary boundary and initial conditions for running the models. Soil moisture estimated through such an approach has been widely recognised and demonstrated in many studies, which cover a broad range of applications from hydrological modelling (Srivastava et al., 2013a;Srivastava et al., 2015), drought studies (Zaitchik et al., 2013), flood investigations (Leung and Qian, 2009), to regional weather prediction (Stéfanon et al., 2014). Therefore, NWP-based soil moisture datasets could provide valuable information for landslide applications. However, to our knowledge, relevant research has never been carried out.

The aim of this study hence is to evaluate the usefulness of NWP modelled soil moisture for landslide monitoring. Here the advanced WRF model (version 3.8) is adopted, because it offers numerous physics options such as micro-physics, surface physics, atmospheric radiation physics, and planetary boundary layer physics (Srivastava et al., 2015), and can integrate with a number of LSM schemes, each varying in physical parameterisation complexities. So far there is limited literature in comparing the soil moisture accuracy of different LSMs options in the WRF model. Therefore, in this study, we select three of the WRF's most advanced LSM schemes (i.e., Noah, Noah-Multiparameterization (Noah-MP), and CLM4) to compare their soil moisture performance for landslide hazard assessment. Furthermore, since all the three schemes can provide multi-layer soil moisture information, it is useful to include all those simulations for the comparison so that the optimal depth of soil moisture could be determined for the landslide monitoring application. The large physiographic variability, plus the abundance of the historical landslide events data, makes Italy a good place for this research. Here an Italian region called Emilia Romagna is selected. The study period covers 10 years from 2006 to 2015 to include a long-term record of landslide events. In addition, because slope angle is a major factor controlling the stability of slope, it is hence used in this study to divide the study area into several slope groups, so that a more accurate threshold model could be built.

The description of the study area and the used datasets are included in Section 2. Methodologies regarding the WRF model, the related LSM schemes and the adopted landslide threshold evaluation approach are provided in Section 3. Section 4 shows the WRF soil moisture evaluation results against the in-situ observations. Section 5 covers the comparison results of the WRF modelled soil moisture products for landslide applications. The discussion and conclusion of the study are included in Section 6.

## 2. Study Area and Datasets

### 2.1 Study Area

The study area is in the Emilia Romagna Region, northern Italy (Figure 1). Its population density is high. The region has high mountainous areas in the S-SW, and wide plain areas towards NE, with a large elevation difference (i.e., 0 m to 2125 m) across 50 km distance from the north to the south. The region has a mild Mediterranean climate with distinct wet and dry seasons (i.e., dry season between May and October, and wet season between November and April). The study area tends to be affected by landslide events easily, with one-fifth of the mountainous zone covered by active or dormant landslide deposits. Rainfall is by far the primary triggering factor of landslides in the region, followed by snow melting: shallow landslides are triggered by short but exceptionally intense rainfall, while deep-seated landslides have a more complex response to rainfall and are mainly caused by moderate but exceptionally prolonged (even up to 6 months) periods of rainfalls (Segoni et al., 2015).

### 2.2 Selection of The Landslide Events

The landslides catalog is collected from the Emilia Romagna Geological Survey (Berti et al., 2012). The information included in the catalog are: location, date of occurrence, the uncertainty of date, landslide characteristics (dimensions, type, and material), triggering factors, damages, casualties, and references. Unfortunately, many of the information are missing from the records in many cases. In order to organise the data in a more systematic way so that only the relevant events are retained, a two-step event selection procedure is initially carried out based on: 1) rainfall-induced only; and

2) high spatial-temporal accuracy (exact date and coordinates). Finally, a revision of the information about the type of slope instabilities such as landslide/debris flow/rockfall and the characteristics of the affected slope (natural or artificial) is also carried out over the selected records (Valenzuela et al., 2018). The catalog period used in this study covers between 2006 and 2015, which is in accordance with the WRF' model run. After filtering the data records, only one-fifths of them (i.e., 157 events) is retained. The retained events are shown as single circles in Figure 2, with slope information (calculated through the Digital Elevation Model (DEM) data) also presented in the background. It can be seen the spatial distribution of the occurred landslide events is very heterogeneous, with nearly all of them occurred in the hilly regions. During the study period, the regional landslide occurrence is mainly dominated by the spatial distribution of the weak earth units and the critical rainfall periods.

### 2.3 Datasets

There is a total of 19 soil moisture stations available within the study area, however only one of them at the San Pietro Capofiume (latitude 44° 39' 13.59", longitude 11° 37' 21.6") provides long-term valid soil moisture retrievals (i.e., 2006 to 2017). We have checked the data from all the rest of the stations, they are either absent (or have very big data gaps) or do not cover the research period at all. Therefore, only the San Pietro Capofiume station is used for the WRF soil moisture temporal evaluation. The soil moisture is measured from 10 cm to 180 cm deep in the soil at 5 depths, by the Time Domain Reflectometry (TDR) instrument. Data are recorded in the unit of volumetric water content ($m^3/m^3$) and at daily timestep (Pistocchi et al., 2008). The data used in this study is between 2006 and 2015. In order to select rainfall events for Year 2014 and 2015, data from 200 tipping-bucket rain gauges are collected and analysed within the region.

To drive a NWP model like WRF for soil moisture simulations, several globally-coved data products can be chosen for extracting the boundary and initial conditions information, for instance, the European Centre for Medium-Range Weather Forecasts (ECMWF) reanalysis (ERA-Interim) and the National Centre for Environmental Prediction (NCEP) reanalysis are two of the most commonly used data products. It has been found by Srivastava et al. (2013b) that the ERA-Interim datasets can provide better boundary conditions than the NCEP datasets for WRF hydro-meteorological predictions in Europe, which is therefore adopted in this study to drive the WRF model. The spatial resolution of the ERA-Interim is approximately 80 km. The data is available from 1979 to present, containing 6-hourly gridded estimates of three-dimensional meteorological variables, and 3-hourly estimates of a large number of surface parameters and other two-dimensional fields. A comprehensive description of the ERA-Interim datasets can be found in (Dee et al., 2011)

The Shuttle Radar Topography Mission (SRTM) 3 Arc-Second Global (~ 90m) DEM datasets is downloaded and used as the basis for the slope degree calculations. SRTM DEM data has been widely used for elevation related studies worldwide due to its high quality, near-global coverage, and free availability (Berry et al., 2007).

## 3. Methodologies

### 3.1 WRF Model and The Three Land Surface Model Schemes

The WRF model is a next-generation, non-hydrostatic mesoscale NWP system designed for both atmospheric research and operational forecasting applications (Skamarock et al., 2005). The model is powerful enough in modelling a broad range of meteorological applications vary from tens of metres to thousands of kilometres (NCAR, 2018). It has two dynamical solvers: the ARW

Hydrol. Earth Syst. Sci. Discuss., https://doi.org/10.5194/hess-2019-95
Manuscript under review for journal Hydrol. Earth Syst. Sci.
Discussion started: 22 March 2019


Hydrology and Earth System Sciences
Open Access
Discussions

(Advanced Research WRF) core and the NMM (Nonhydrostatic Mesoscale Model) core. The former has more complex dynamic and physics settings than the latter which only has limited setting choices. Hence in this study WRF with ARW dynamic core (version 3.8) is used to perform all the soil moisture simulations.

The main task of LSM within the WRF is to integrate information generated through the surface layer scheme, the radiative forcing from the radiation scheme, the precipitation forcing from the microphysics and convective schemes, and the land surface conditions to simulate the water and energy fluxes (Ek et al., 2003). WRF provides several LSM options, among which three of them are selected in this study as mentioned in the introduction: Noah, Noah-MP, and CLM4. Table 1 gives a simple comparison of the three models. The detailed description of the models is written below in the order of increasing complexity in regards of the way they deal with thermal and moisture fluxes in various layers of soil, and their vegetation, root and canopy effects (Skamarock et al., 2008).

**3.1.1 Noah**

Noah is the most basic amongst the three selected LSMs. It is one of the 'second generation' LSMs that relies on both soil and vegetation processes for water budgets and surface energy closures (Wei et al., 2010). The model is capable of modelling soil and land surface temperature, snow water equivalent, as well as the general water and energy fluxes. The model includes four soil layers that reach a total depth of 2 m in which soil moisture is calculated. Its bulk layer of canopy -snow-soil (i.e., lack the abilities in simulating photosynthetically active radiation (PAR), vegetation temperature, correlated energy, and water, heat and carbon fluxes), 'leaky' bottom (i.e., drained water is removed immediately from the bottom of the soil column which can result in much fewer memories of antecedent weather and climate fluctuations) and simple snow melt-thaw dynamics are seen as the model's demerits (Wharton et al., 2013). Noah calculates the soil moisture from the diffusive form of Richard's equation for each of the soil layer (Greve et al., 2013), and the evapotranspiration from the Ball-Berry equation (considering both the water flow mechanism within soil column and vegetation, as well as the physiology of photosynthesis (Wharton et al., 2013)).

### 3.1.2 Noah-MP

Noah-MP (Niu et al., 2011) is an improved version of the Noah LSM, in the aspect of better representations of terrestrial biophysical and hydrological processes. Major physical mechanism improvements directly relevant to soil water simulations include: 1) introducing a more permeable frozen soil by separating permeable and impermeable fractions (Cai, 2015), 2) adding an unconfined aquifer immediately beneath the bottom of the soil column to allow the exchange of water between them (Liang et al., 2003), and 3) the adoption of a TOPMODEL (TOPography based hydrological MODEL)-based runoff scheme (Niu et al., 2005) and a simple SIMGM groundwater model (Niu et al., 2007) which are both important in improving the modelling of soil hydrology. Noah-MP is unique compared with the other LSMs, as it is capable of generating thousands of parameterisation schemes through the different combinations of "dynamic leaf, canopy stomatal resistance, runoff and groundwater, a soil moisture factor controlling stomatal resistance (the β factor), and six other processes" (Cai, 2015). The scheme option used in the study are: Ball-Berry scheme for canopy stomatal resistance, Monin-Obukhov scheme for surface layer drag coefficient calculation, the Noah based soil moisture factor for stomatal resistance, the TOPMODEL runoff with the SIMGM groundwater, the linear effect scheme for soil permeability, the two-stream applied to vegetated fraction scheme for radiative transfer, the CLASS (Canadian

Land Surface Scheme) scheme for ground surface albedo option, and the Jordan (Jordan, 1991) scheme for partitioning precipitation between snow and rain.

#### 3.1.3. CLM4

CLM4 is developed by the National Center for Atmospheric Research (NCAR) to serve as the land component of its Community Earth System Model (formerly known as the Community Climate System Model) (Lawrence et al., 2012). It is a 'third generation' model that incorporates the interactions of both nitrogen and carbon in the calculations of water and energy fluxes. Compared with its previous versions, CLM4 (Oleson et al., 2008) has multiple enhancements relevant to soil moisture computing. For instance, the model's soil moisture is estimated by adopting a improved one-dimensional Richards equation (Zeng and Decker, 2009); the new version allows the dynamic interchanges of soil water and groundwater through an improved definition of the soil column's lower boundary condition that is similar to the Noah-MP's (Niu et al., 2007). Furthermore, the thermal and hydrologic properties of organic soil are included for the modelling which is based on the method developed in (Lawrence and Slater, 2008). The total ground column is extended to 42 m depth, consisting 10 soil layers unevenly spaced between the top layer (0.0–1.8 cm) and the bottom layers (229.6–380.2 cm), and 5 bedrock layers to the bottom of the ground column (Lawrence et al., 2011). Soil moisture is estimated for each soil layer.

### 3.2 WRF Model Parameterization

The WRF model is centred over the Emilia Romagna Region with three nested domains (D1, D2, D3 with the horizontal grid sizes of 45 km, 15 km, and 5 km, respectively), of which the innermost domain (D3, with 88 x 52 grids (west-east and south-north, respectively)) is used in this study. A two-way nesting scheme is adopted allowing information from the child domain to be fed back to

Hydrol. Earth Syst. Sci. Discuss., https://doi.org/10.5194/hess-2019-95
Manuscript under review for journal Hydrol. Earth Syst. Sci.
Discussion started: 22 March 2019


Hydrology and Earth System Sciences
Open Access
Discussions

the parent domain. With atmospheric forcing, static inputs (e.g., soil and vegetation types), and parameters, the WRF model needs to be spun-up to reach its equilibrium state before it can be used (Cai et al., 2014;Cai, 2015). In this study, WRF is spun-up by running through the whole year of 2005. After spin-up, the WRF model for each of the selected LSM scheme is executed in daily timestep from January 1, 2006, to December 31, 2015, using the ERA-Interim datasets.

The microphysics scheme plays a vital role in simulating accurate rainfall information which in turn is important for modelling the accurate soil moisture variations. WRF V3.8 is supporting 23 microphysics options range from simple to more sophisticated mixed-phase physical options. In this study, the WRF Single-Moment 6-class scheme is adopted which considers ice, snow and graupel processes and is suitable for high-resolution applications (Zaidi and Gisen, 2018). The physical options used in the WRF setup are Dudhia shortwave radiation (Dudhia, 1989) and Rapid Radiative Transfer Model (RRTM) longwave radiation (Mlawer et al., 1997). Cumulus parameterization is based on the Kain-Fritsch scheme (Kain, 2004) which is capable of representing sub-grid scale features of the updraft and rain processes, and such a capability is beneficial for real-time modelling (Gilliland and Rowe, 2007). The surface layer parameterization is based on the Revised fifth-generation Pennsylvania State University–National Center for Atmospheric Research Mesoscale Model (MM5) Monin-Obukhov scheme (Jiménez et al., 2012). The Yonsei University scheme (Hong et al., 2006) is selected to calculate the planetary boundary layer. The parameterization schemes used in the WRF modelling are shown in Table 2. The datasets for land use and soil texture are available in the pre-processing package of WRF. In this study, the land use categorisation is interpolated from the MODIS 21-category data classified by the International Geosphere Biosphere Programme (IGBP). The soil texture data are based on the Food and Agriculture Organization of the United Nations Global 5-minutes soil database.

### 3.3 Translation of Observed and Simulated Soil Moisture Data to Common Soil Layers

Since all soil moisture datasets have different soil depths, it is difficult for a direct comparison. The Noah and Noah-MP models include four soil layers, centred at 5, 25, 70, and 150 cm, respectively. Whereas CLM4 model has 10 soil layers, centered at 0.9, 3.2, 6.85, 12.85, 22.8, 39.2, 66.2, 110.65, 183.95, 304.9 cm, respectively. Moreover, the in-situ sensor measures soil moisture centred at 10, 25, 70, 135, and 180 cm. In order to tackle the inconsistency issue of soil depths, the simple linear interpolation approach described in Zhuo et al. (2015b) is applied in this study, and a benchmark of soil layer centred at 10, 25, 70 and 150 cm is adopted.

### 3.4 Soil Moisture Thresholds Build Up and Evaluations

To build and evaluate the soil moisture thresholds for landslides forecasting, all datasets have been grouped into two portions: 2006-2013 for the establishment of thresholds, and 2014-2015 for the evaluation. The determination of soil moisture thresholds is based on determining the most suitable soil moisture triggering level for landslides occurrence by trying a range of exceedance probabilities (percentiles). For example, a 10% exceedance probability is calculated by determining the 10% percentile result of the soil moisture datasets that is related to the occurred landslides. The exceedance probability method is commonly utilised in landslide early warning studies for calculating the rainfall-thresholds, which is therefore adopted here to examine its performance for soil moisture threshold calculations.

To carry out the threshold evaluation, 45 rainfall events (during 2014-2015) are selected for the purpose. The rainfall events are separated based on at least one-day of dry period (i.e., a period without rainfall) (Dai et al., 2014;Dai et al., 2015;Dai et al., 2016). The rainfall data from each rain gauge station is firstly combined using the Thiessen Polygon method, and with visual analysis, the

Hydrol. Earth Syst. Sci. Discuss., https://doi.org/10.5194/hess-2019-95
Manuscript under review for journal Hydrol. Earth Syst. Sci.
Discussion started: 22 March 2019


Hydrology and Earth System Sciences
Open Access
Discussions

45 events are then finally selected. The information about the selected rainfall events can be found in Section 5. The threshold evaluation is based on the statistical approach described in Gariano et al. (2015) and Zhuo et al. (2019), where soil moisture threshold can be treated as a binary classifier of the soil moisture conditions that are likely or unlikely to cause landslide events. With this hypothesis, the likelihood of a landslide event can either be *true* (*T*) or *false* (*F*), and the threshold forecasting can either be *positive* (*P*) or *negative* (*N*). The combinations of those four conditions can lead to four statistical outcomes (Figure 3a) that are: *true positive* (*TP*), *true negative* (*TN*), *false positive* (*FP*), and *false negative* (*FN*) (Wilks, 2011). The detailed description of each outcome is covered in Zhuo et al. (2019). Using the four outcomes, two statistical scores can be determined.

The Hit Rate (*HR*), which is the rate of the events that are correctly forecasted. Its formula is:

$$HR = \frac{TP}{TP+FN} \tag{1}$$

in the range of 0 and 1, with the best result as 1.

The False Alarm Rate (*FAR*), which is the rate of false alarms when the event did not occur. Its formula is:

$$FAR = \frac{FP}{FP+TN} \tag{2}$$

in the range of 0 and 1, with the best result as 0.

For any soil moisture product, each threshold calculated for each of the slope degree group is adopted to determine *T*, *F*, *P*, and *N*, respectively. Those values are finally integrated to find the overall scores of *TP*, *FN*, *FP*, *TN*, *HR*, and *FAR*. The threshold performance is then judged via the Receiver Operating Characteristic (ROC) analysis (Hosmer and Lemeshow, 1989;Fawcett, 2006). As shown in Figure 3b, ROC curve is based on *HR* against *FAR*, and each point in the curve represents a threshold scenario (i.e., selected exceedance probabilities). The optimal result (the red point) can only be realised when the *HR* reaches 1 and the *FAR* reduces to 0. The closer the point

Hydrol. Earth Syst. Sci. Discuss., https://doi.org/10.5194/hess-2019-95
Manuscript under review for journal Hydrol. Earth Syst. Sci.
Discussion started: 22 March 2019

Hydrology and Earth System Sciences
Open Access
Discussions

to the red point, the better the forecasting result is. To analyse and compare the forecasting performance numerically, the Euclidean distances (*d*) for each scenario to the optimal point are computed.

## 4. WRF Soil Moisture Analysis and Evaluations

### 4.1 Temporal Comparisons

Although there is only one soil moisture sensor that provides long-term soil moisture data in the study region, it is still useful to compare it with the WRF estimated soil moisture. Particularly, it has been shown that soil moisture measured at a site location can reflect the temporal fluctuations of soil moisture for its surrounding region, up to 500 km in radius (Entin et al., 2000). With the WRF's relatively high-resolution of 5 km, the temporal comparison with the in-situ observations should provide some meaningful results. In this study, we carry out a temporal comparison between all the three WRF soil moisture products with the in-situ observations. The comparison is implemented over the period from 2006 to 2015, and the WRF grid closest to the in-situ sensor location is chosen. Figure 4 shows the comparison results at the four soil depths. The statistical performance (correlation coefficient *r* and Root Mean Square Error *RMSE*) of the three LSM schemes are summarised in Table 3. Based on the statistical results, Noah-MP surpasses other schemes at most soil layers, except for layer 2 where CLM4 shows stronger correlation and layer 4 where Noah gives smaller *RMSE* error. For Noah-MP, the best correlation is observed at the surface layer (0.809), followed by third (0.738), second (0.683) and fourth (0.498) layers; and based on *RMSE*, the best performance is again observed at the surface layer and followed by second, third and fourth layers in sequence (as 0.060, 0.070, 0.088, and 0.092 $m^3/m^3$, respectively). From the temporal plots, it can be seen at all four soil layers, all three LSM schemes can produce

Hydrol. Earth Syst. Sci. Discuss., https://doi.org/10.5194/hess-2019-95
Manuscript under review for journal Hydrol. Earth Syst. Sci.
Discussion started: 22 March 2019




soil moisture's seasonal cycle very well with most upward and downward trends successfully represented. However, both the Noah and the CLM4 overestimate the variability at the upper two soil layers during almost the whole study period, and the situation is the worst for the Noah. Comparatively, the Noah-MP can capture the wet soil moisture conditions very well especially at the surface layer; and it is the only model of the three that is able to simulate the large soil drying phenomenon close to the observations during the dry season, except for some extremely dry days. Towards 70 cm depth, although Noah-MP is still able to capture most of the soil moisture variabilities during the drying period, it significantly underestimates soil moisture values for most wet days. Similar underestimation results can be observed for CLM4 and Noah during the wet season at 70 cm; furthermore, both schemes are again not capable of reproducing the extremely drying phenomenon and overestimate soil moisture for most of the dry season days. It is surprising to see that at the deep soil layer (150 cm), all soil moisture products are underestimated, in particular, the outputs from the CLM4 and the Noah-MP only show small fluctuations. However, the soil moisture measurements from the in-situ sensor also get our attention as they show strange fluctuations with numerous sudden drops and rise situations observed. The strange phenomenon is not expected at such a deep soil layer (although groundwater capillary forces can increase the soil moisture, its rate is normally very slow). One possible reason we suspect is due to sensor failure in the deep zone. Overall for the Noah-MP, in addition to producing the highest correlation coefficient and the lowest *RMSE*, its simulated soil moisture variations are the closest to the observations. The better performance of the Noah-MP over the other two models agrees with the results found in Cai et al. (2014) (note: the paper uses standalone models, which are not coupled with WRF). Also, it has been discussed in Yang et al. (2011), the Noah MP presents a clear improvement over the Noah in simulating soil moisture globally.

Hydrol. Earth Syst. Sci. Discuss., https://doi.org/10.5194/hess-2019-95
Manuscript under review for journal Hydrol. Earth Syst. Sci.
Discussion started: 22 March 2019



**4.2 Spatial Comparisons**

Figure 5, 6 shows the spatial distribution of soil moisture simulations (via the three WRF LSM schemes) at the four soil layers on a typical day during the dry and the wet seasons, respectively. It is clear to see on the dry season day, Noah gives the wettest soil moisture simulation amongst the three schemes, followed by CLM4 and Noah-MP. The soil moisture spatial pattern of the three schemes more or less agrees with each, that is with wetter soil condition found in the central (in line with the location of the river mainstream) and South-West part of the study region and dryer soil condition in the Southern boundary and East part of the study region. On the wet season day, Noah again produces wetter soil moisture data than the other two schemes, and it shows a distinct wet patch at the Southern boundary while both the Noah-MP and the CLM4's simulations indicate that part as the driest of the whole region. The disagreement among the LSMs at the Southern boundary could be due to the particularly high elevation (above 2000 m) and snow existence at that region, and the three schemes use different theories to deal with such conditions. The improvement in the Noah-MP and the CLM4 is mainly attributed to the better simulation of snow, in particular, it has been found Noah-MP can better simulate the snowmelt phenomenon over the other two schemes (Cai et al., 2014), because it has better representations of ground heat flux, retention, percolation and refreezing of melted liquid water within the multilayer snowpack (Yang et al., 2011). Furthermore, it can be seen Noah-MP has a clear spatial pattern of the soil moisture in the region, that is with drier areas found near the river mainstream, and Southern boundary, and wetter zones in the North and the South. On the contrary, Noah and CLM4 simulated soil moisture show a relatively smaller difference spatially, especially for CLM4.

**5. The Assessment of WRF Soil Moisture Threshold for Landslide Monitoring**

This section is to assess if the spatial distribution of soil moisture can provide useful information for landslide monitoring at the regional scale. Particularly, all three soil moisture products simulated through the WRF model are used to derive threshold models, and the corresponding landslide prediction performances are then compared statistically. Here the threshold is defined as the crucial soil moisture condition above which landslides are likely to happen.

Among different factors for controlling the stability of slope, the slope angle is one of the most critical ones. From the slope angle map in Figure 2, it can be seen the region has a clear spatial pattern of high and low slope areas, with the majority of the high-slope areas (can be as steep as around 40 degrees) located in the mountainous Southern part and the river valleys. Moreover, there is an obvious causal relationship between the slope angle and the landslide occurrence, as all the landslides happened during the study period are located in the high-slope region, with a particularly high concentration around the central Southern part. The spatial distribution of the landslide events is also in line with the overall geological characteristics of the region, i.e., the Southern part mainly constitutes outcrop of sandstone rocks that make up the steep slopes and are covered by a thin layer of permeable sandy soil, which are highly unstable (Zhuo et al., 2019). Therefore, instead of only using one soil moisture threshold for the whole study area, it is useful to divide the region into several slope groups so that within each group a threshold model is built. To derive soil moisture threshold individually under different slope conditions, all data has been divided into three groups based on the slope angle (0.4-1.86$^o$; 1.87-9.61$^o$; 9.52-40.43$^o$; since no landslide events are recorded under the 0-0.39$^o$ group, the group is not considered here), as results, all groups have equal coverage areas.

In order to find the optimal threshold so that there are least missing alarms (i.e., threshold is overestimated) and false alarms (i.e., threshold is underestimated), we test out 17 different

Hydrol. Earth Syst. Sci. Discuss., https://doi.org/10.5194/hess-2019-95
Manuscript under review for journal Hydrol. Earth Syst. Sci.
Discussion started: 22 March 2019


exceedance probabilities from 1% to 50%. For each LSM scheme, the total number of threshold models is 204, which is the resultant of different combinations of slope groups, soil layers, and exceedance probability conditions. The calculated thresholds for all LSM schemes under three slope groups are plotted in Figure 7. Overall there is a very clear trend between the slope angle and the soil moisture threshold, that is with threshold becoming smaller for steeper areas. The correlation is particularly evident at the upper three soil layers (i.e., the top 1 m depth of soil), with only a few exceptions for Noah and CLM4 at the 1% and the 2% exceedance probabilities. At the deep soil layer centred at 150 cm, the soil moisture threshold difference between Slope Group (S.G.) 2 and 3 becomes very small for all the three LSM schemes. This could be partially because at the deep soil layer, the change of soil moisture is much smaller than at the surface layer, therefore the soil moisture values for S.G. 2 and 3 could be too similar to differentiate. However, for milder slopes (S.G. 1), the higher soil moisture triggering level always applies even down to the deepest soil layer for all the three LSM schemes. It is also clear to see the difference of threshold values amongst different slope groups largely depends on the number of landslide events considered, that is with more events considered, the stronger the correlation (e.g., 1% exceedance probability means 99% of the events are included for the threshold modelling, whilst 50% exceedance probability means half of the data are treated as outliers). The results confirm that wetter soil indeed can trigger shallow landslides easier in milder slopes than in steeper slopes.

All the threshold models are then evaluated under the 45 selected rainfall events (Table 4) using the ROC analysis. The period of the selected rainfall events is between 1 day and 18 days, and the average rainfall intensity ranges from 5.05 mm/day to 24.69 mm/day. For each selected event, the number of landslide event is also summarised in the table. The resultant Euclidean distances (*d*) between each scenario of exceedance probability and the optimal point for ROC analysis are listed in Table 5 for all three WRF LSM schemes at the tested exceedance probabilities. The best performance (i.e., lowest $d$) in each column (i.e., each soil layer of an LSM scheme) is highlighted. In addition, the $d$ results are also plotted in Figure 8 to give a better view of the overall trend amongst different soil layers and LSM schemes. From the figure, for all three LSM schemes at all four soil layers, there is an overall downward and then stabilised trend. Overall for Noah, the simulated surface layer soil moisture provides better landslide monitoring performance than the rest of the soil layers from 1% to 35% exceedance probabilities; and the scheme's worst performance is observed at the third soil layer centred at 70 cm. The values of $d$ for Noah's second and fourth layer are quite close to each other. For Noah-MP, the simulated surface layer soil moisture gives the best performance amongst all four soil layers for most cases between the 1% and 35% exceedance probability range; and the scheme's worst performance is observed at the fourth layer. Unlike Noah, all four soil layers from the Noah-MP scheme provide distinct performance amongst them (i.e., larger $d$ difference). For CLM4, the performance for the surface layer is quite similar to the second layer's, and the differences amongst the four layers are small. From the Table 5, it can be seen for Noah the most suitable exceedance probabilities (i.e., the highlighted numbers) range between 35% to 50%; for Noah-MP they are between 30% and 50%; and for CLM4 it stays at 40% for all four soil layers. For both Noah and Noah-MP, the best performance is observed at the surface layer ($d$ = 0.392 and $d$ = 0.369, respectively), which is in line with their correlation coefficient results against the in-situ observations (i.e., the best $r$ value for both LSM schemes is found at the surface layer). Furthermore, the best performance for Noah and Noah-MP follows a regular trend, that is the deeper the soil layer, the poorer the landslide monitoring performance. For CLM4, the best performances show no distinct pattern amongst soil layers (i.e., with the best performance found at the soil layer 3, followed by layer 2, 1, and 4). Of all the LSM schemes and soil layers, the best performance is found for Noah-MP at the surface layer with 30% exceedance probability ($d$=0.369). The ROC curve for the Noah-MP scheme at the surface layer is shown in Figure 9. In the curve, each point represents a scenario with a selected exceedance probability level. It is clear with various exceedance probabilities, *FAR* can be decreased without sacrificing the *HR* score (e.g., 4% to 10% exceedance probabilities). At the optimal point at the 30% exceedance probability, the best results for *HR* and *FAR* are observed as 0.769 and 0.289, respectively.

## 6. Discussions and Conclusion

In this study, the usability of WRF modelled soil moisture for landslide monitoring has been evaluated in the Emilia Romagna region based on the research duration between 2006 and 2015. Specifically, four-layer soil moisture information simulated through the WRF's three most advanced LSM schemes (i.e., Noah, Noah-MP and CLM4) are compared for the purpose. Through the temporal comparison with the in-situ soil moisture observations, it has been found that all three LSM schemes at all four soil layers can produce soil moisture's seasonal cycle very well. However, only Noah-MP is able to simulate the large soil drying phenomenon close to the observations during the drying season, and it also gives the highest correlation coefficient and the lowest *RMSE* at most soil layers amongst the three LSM schemes. For landslide threshold build up, slope information is useful in identifying threshold differences, with threshold becoming smaller for steeper area. In other words, dryer soil indeed can trigger landslides in steeper slopes than in milder slopes. The result is not surprising, as the slope angle is an importance element of influencing the stabilities of earth materials. Further studies based on slope angle condition is then carried out. 17 various exceedance probably levels between 1% and 50% are adopted to find the optimal threshold scenario. Through the ROC analysis of 612 threshold models, the best performance is obtained by the Noah-MP at the surface soil layer with 30% exceedance probability. The outstanding performance of the Noah-MP scheme at the surface layer is also in accordance with its high correlation coefficient result found against the in-situ observations.

It should be noted that weighting factors are not considered in the evaluation of the threshold models. Nevertheless, in real-life situations, weighting could play important roles during the final decision making. As for instance, the damages resulted from a missing alarm event could be much more devastating than a false alarm event, or vice versa, and the situation also varies in different regions. Therefore, during operational applications, weighting factors should be considered.

Model-based soil moisture estimations could be affected by error accumulation issues, especially in the real-time forecasting mode. A potential solution is to use data assimilation methodologies to correct such errors by intaking soil moisture information from other data sources. Since in-situ soil moisture sensors are only sparsely available in limited regions, soil moisture measured via satellite remote sensing technologies could provide useful alternatives. Another issue is with the landslide record data, since most of them are based on human experiences (e.g., through newspapers, and victims), a lot of incidences could be unreported. Therefore, the conclusion made here could be biased. One way of expanding the current landslide catalog can depend on automatic landslide detection methods based on remote sensing images.

In summary, this study gives an overview of the soil moisture performance of three WRF LSM schemes for landslide hazard assessment. We demonstrate that the surface soil moisture (centred at 10 cm) simulated through the Noah-MP LSM scheme is useful in predicting landslide occurrences in the Emelia Romagna region. The high hitting rate of 0.769 and the low false alarm rate of 0.289 obtained in this study show such valuable soil moisture information could work in addition to the rainfall data to provide an efficient landslide early warning system at the regional scales. However, one must bear in mind that the results demonstrated in this study are only valid for the selected region. In order to make a general conclusion, more researches are needed. Particularly, a considerable number of catchments with a broad spectrum of climate and environmental conditions will need to be investigated.

## Acknowledgement

This study is supported by Resilient Economy and Society by Integrated SysTems modelling (RESIST), Newton Fund via Natural Environment Research Council (NERC) and Economic and Social Research Council (ESRC) (NE/N012143/1), and the National Natural Science Foundation of China (No：4151101234).

## References

Baum, R. L., and Godt, J. W.: Early warning of rainfall-induced shallow landslides and debris flows in the USA, Landslides, 7, 259-272, 2010.

Berry, P., Garlick, J., and Smith, R.: Near-global validation of the SRTM DEM using satellite radar altimetry, Remote Sensing of Environment, 106, 17-27, 2007.

Berti, M., Martina, M., Franceschini, S., Pignone, S., Simoni, A., and Pizziolo, M.: Probabilistic rainfall thresholds for landslide occurrence using a Bayesian approach, Journal of Geophysical Research: Earth Surface, 117, 2012.

Bittelli, M., Valentino, R., Salvatorelli, F., and Pisa, P. R.: Monitoring soil-water and displacement conditions leading to landslide occurrence in partially saturated clays, Geomorphology, 173, 161-173, 2012.

Hydrol. Earth Syst. Sci. Discuss., https://doi.org/10.5194/hess-2019-95
Manuscript under review for journal Hydrol. Earth Syst. Sci.
Discussion started: 22 March 2019


Bogaard, T., and Greco, R.: Invited perspectives: Hydrological perspectives on precipitation intensity-duration thresholds for landslide initiation: proposing hydro-meteorological thresholds, Natural Hazards and Earth System Sciences, 18, 31-39, 2018.

Brocca, L., Melone, F., and Moramarco, T.: On the estimation of antecedent wetness conditions in rainfall–runoff modelling, Hydrological Processes: An International Journal, 22, 629-642, 2008.

Cai, X., Yang, Z. L., Xia, Y., Huang, M., Wei, H., Leung, L. R., and Ek, M. B.: Assessment of simulated water balance from Noah, Noah-MP, CLM, and VIC over CONUS using the NLDAS test bed, Journal of Geophysical Research: Atmospheres, 119, 13,751-713,770, 2014.

Cai, X.: Hydrological assessment and biogeochemical advancement of the Noah-MP land surface model, 2015.

Caine, N.: The rainfall intensity-duration control of shallow landslides and debris flows, Geografiska annaler: series A, physical geography, 62, 23-27, 1980.

Calvello, M., d'Orsi, R. N., Piciullo, L., Paes, N., Magalhaes, M., and Lacerda, W. A.: The Rio de Janeiro early warning system for rainfall-induced landslides: analysis of performance for the years 2010–2013, International journal of disaster risk reduction, 12, 3-15, 2015.

Chae, B.-G., Park, H.-J., Catani, F., Simoni, A., and Berti, M.: Landslide prediction, monitoring and early warning: a concise review of state-of-the-art, Geosciences Journal, 21, 1033-1070, 2017.

Chen, F., and Dudhia, J.: Coupling an advanced land surface-hydrology model with the Penn State-NCAR MM5 modeling system. Part I: Model implementation and sensitivity, Monthly Weather Review, 129, 569-585, 2001.

Chleborad, A. F.: Preliminary evaluation of a precipitation threshold for anticipating the occurrence of landslides in the Seattle, Washington, Area, US Geological Survey open-file report, 3, 39, 2003.

Crozier, M. J.: Prediction of rainfall-triggered landslides: A test of the antecedent water status model, Earth surface processes and landforms, 24, 825-833, 1999.

Dai, Q., Han, D., Rico-Ramirez, M., and Srivastava, P. K.: Multivariate distributed ensemble generator: A new scheme for ensemble radar precipitation estimation over temperate maritime climate, Journal of Hydrology, 511, 17-27, 2014.

Dai, Q., Han, D., Rico-Ramirez, M. A., Zhuo, L., Nanding, N., and Islam, T.: Radar rainfall uncertainty modelling influenced by wind, Hydrological processes, 29, 1704-1716, 2015.

Dai, Q., Han, D., Zhuo, L., Zhang, J., Islam, T., and Srivastava, P. K.: Seasonal ensemble generator for radar rainfall using copula and autoregressive model, Stochastic environmental research and risk assessment, 30, 27-38, 2016.

Dee, D. P., Uppala, S. M., Simmons, A., Berrisford, P., Poli, P., Kobayashi, S., Andrae, U., Balmaseda, M., Balsamo, G., and Bauer, d. P.: The ERA-Interim reanalysis: Configuration and performance of the data assimilation system, Quarterly Journal of the royal meteorological society, 137, 553-597, 2011.

Dudhia, J.: Numerical study of convection observed during the winter monsoon experiment using a mesoscale two-dimensional model, Journal of the Atmospheric Sciences, 46, 3077-3107, 1989.

Ek, M., Mitchell, K., Lin, Y., Rogers, E., Grunmann, P., Koren, V., Gayno, G., and Tarpley, J.: Implementation of Noah land surface model advances in the National Centers for Environmental

Hydrol. Earth Syst. Sci. Discuss., https://doi.org/10.5194/hess-2019-95
Manuscript under review for journal Hydrol. Earth Syst. Sci.
Discussion started: 22 March 2019


Prediction operational mesoscale Eta model, Journal of Geophysical Research: Atmospheres, 108, 2003.

Entin, J. K., Robock, A., Vinnikov, K. Y., Hollinger, S. E., Liu, S., and Namkhai, A.: Temporal and spatial scales of observed soil moisture variations in the extratropics, Journal of Geophysical Research: Atmospheres, 105, 11865-11877, 2000.

Fawcett, T.: An introduction to ROC analysis, Pattern recognition letters, 27, 861-874, 2006.

Froude, M. J., and Petley, D.: Global fatal landslide occurrence from 2004 to 2016, Natural Hazards and Earth System Sciences, 18, 2161-2181, 2018.

Gariano, S. L., Brunetti, M. T., Iovine, G., Melillo, M., Peruccacci, S., Terranova, O., Vennari, C., and Guzzetti, F.: Calibration and validation of rainfall thresholds for shallow landslide forecasting in Sicily, southern Italy, Geomorphology, 228, 653-665, 2015.

Gariano, S. L., and Guzzetti, F.: Landslides in a changing climate, Earth-Science Reviews, 162, 227-252, 2016.

Gilliland, E. K., and Rowe, C. M.: A comparison of cumulus parameterization schemes in the WRF model, Proceedings of the 87th AMS Annual Meeting & 21th Conference on Hydrology, 2007,

Glade, T., Crozier, M., and Smith, P.: Applying probability determination to refine landslide-triggering rainfall thresholds using an empirical “Antecedent Daily Rainfall Model”, Pure and Applied Geophysics, 157, 1059-1079, 2000.

Greco, R., Guida, A., Damiano, E., and Olivares, L.: Soil water content and suction monitoring in model slopes for shallow flowslides early warning applications, Physics and Chemistry of the Earth, Parts A/B/C, 35, 127-136, 2010.

Greve, P., Warrach-Sagi, K., and Wulfmeyer, V.: Evaluating soil water content in a WRF-Noah downscaling experiment, Journal of Applied Meteorology and Climatology, 52, 2312-2327, 2013.

Harris, S., Orense, R., and Itoh, K.: Back analyses of rainfall-induced slope failure in Northland Allochthon formation, Landslides, 9, 349-356, 2012.

Hawke, R., and McConchie, J.: In situ measurement of soil moisture and pore-water pressures in an 'incipient'landslide: Lake Tutira, New Zealand, Journal of environmental management, 92, 266-274, 2011.

Hong, S.-Y., Noh, Y., and Dudhia, J.: A new vertical diffusion package with an explicit treatment of entrainment processes, Monthly Weather Review, 134, 2318-2341, 2006.

Hosmer, D., and Lemeshow, S.: Applied logistic regression. 1989, New York: Johns Wiley & Sons, 1989.

Jiménez, P. A., Dudhia, J., González-Rouco, J. F., Navarro, J., Montávez, J. P., and García-Bustamante, E.: A revised scheme for the WRF surface layer formulation, Monthly Weather Review, 140, 898-918, 2012.

Jordan, R.: A one-dimensional temperature model for a snow cover: Technical documentation for SNTHERM. 89, COLD REGIONS RESEARCH AND ENGINEERING LAB HANOVER NH, 1991.

Hydrol. Earth Syst. Sci. Discuss., https://doi.org/10.5194/hess-2019-95
Manuscript under review for journal Hydrol. Earth Syst. Sci.
Discussion started: 22 March 2019


Kain, J. S.: The Kain-Fritsch convective parameterization: An update, Journal of Applied Meteorology, 43, http://dx.doi.org/10.1175/1520-0450(2004)043<0170:TKCPAU>2.0.CO;2, 2004.

Klose, M., Highland, L., Damm, B., and Terhorst, B.: Estimation of Direct Landslide Costs in Industrialized Countries: Challenges, Concepts, and Case Study, in: Landslide Science for a Safer Geoenvironment, World Landslide Forum 3, China (Beijing), 2014, 661-667,

Lawrence, D. M., and Slater, A. G.: Incorporating organic soil into a global climate model, Climate Dynamics, 30, 145-160, 2008.

Lawrence, D. M., Oleson, K. W., Flanner, M. G., Thornton, P. E., Swenson, S. C., Lawrence, P. J., Zeng, X., Yang, Z. L., Levis, S., and Sakaguchi, K.: Parameterization improvements and functional and structural advances in version 4 of the Community Land Model, Journal of Advances in Modeling Earth Systems, 3, 2011.

Lawrence, D. M., Oleson, K. W., Flanner, M. G., Fletcher, C. G., Lawrence, P. J., Levis, S., Swenson, S. C., and Bonan, G. B.: The CCSM4 land simulation, 1850–2005: Assessment of surface climate and new capabilities, Journal of Climate, 25, 2240-2260, 2012.

Leung, L. R., and Qian, Y.: Atmospheric rivers induced heavy precipitation and flooding in the western US simulated by the WRF regional climate model, Geophysical research letters, 36, 2009.

Liang, X., Xie, Z., and Huang, M.: A new parameterization for surface and groundwater interactions and its impact on water budgets with the variable infiltration capacity (VIC) land surface model, Journal of Geophysical Research: Atmospheres, 108, 2003.

Maheu, A., Anctil, F., Gaborit, É., Fortin, V., Nadeau, D. F., and Therrien, R.: A field evaluation of soil moisture modelling with the Soil, Vegetation, and Snow (SVS) land surface model using evapotranspiration observations as forcing data, Journal of Hydrology, 558, 532-545, 2018.

Mlawer, E. J., Taubman, S. J., Brown, P. D., Iacono, M. J., and Clough, S. A.: Radiative transfer for inhomogeneous atmospheres: RRTM, a validated correlated-k model for the longwave, Journal of Geophysical Research: Atmospheres, 102, 16663-16682, 1997.

Weather research and forcasting model, 2018.

Niu, G. Y., Yang, Z. L., Dickinson, R. E., and Gulden, L. E.: A simple TOPMODEL-based runoff parameterization (SIMTOP) for use in global climate models, Journal of Geophysical Research: Atmospheres, 110, 2005.

Niu, G. Y., Yang, Z. L., Dickinson, R. E., Gulden, L. E., and Su, H.: Development of a simple groundwater model for use in climate models and evaluation with Gravity Recovery and Climate Experiment data, Journal of Geophysical Research: Atmospheres, 112, 2007.

Niu, G. Y., Yang, Z. L., Mitchell, K. E., Chen, F., Ek, M. B., Barlage, M., Kumar, A., Manning, K., Niyogi, D., and Rosero, E.: The community Noah land surface model with multiparameterization options (Noah-MP): 1. Model description and evaluation with local-scale measurements, Journal of Geophysical Research: Atmospheres, 116, 2011.

Oleson, K., Niu, G. Y., Yang, Z. L., Lawrence, D., Thornton, P., Lawrence, P., Stöckli, R., Dickinson, R., Bonan, G., and Levis, S.: Improvements to the Community Land Model and their impact on the hydrological cycle, Journal of Geophysical Research: Biogeosciences (2005–2012), 113, 2008.

Hydrol. Earth Syst. Sci. Discuss., https://doi.org/10.5194/hess-2019-95
Manuscript under review for journal Hydrol. Earth Syst. Sci.
Discussion started: 22 March 2019


Oleson, K. W., Lawrence, D. M., Gordon, B., Flanner, M. G., Kluzek, E., Peter, J., Levis, S., Swenson, S. C., Thornton, E., and Feddema, J.: Technical description of version 4.0 of the Community Land Model (CLM), 2010.

Pelletier, J. D., Malamud, B. D., Blodgett, T., and Turcotte, D. L.: Scale-invariance of soil moisture variability and its implications for the frequency-size distribution of landslides, Engineering Geology, 48, 255-268, 1997.

Petley, D.: Global patterns of loss of life from landslides, Geology, 40, 927-930, 2012.

Pistocchi, A., Bouraoui, F., and Bittelli, M.: A simplified parameterization of the monthly topsoil water budget, Water Resources Research, 44, 2008.

Posner, A. J., and Georgakakos, K. P.: Soil moisture and precipitation thresholds for real-time landslide prediction in El Salvador, Landslides, 12, 1179-1196, 2015.

Segoni, S., Lagomarsino, D., Fanti, R., Moretti, S., and Casagli, N.: Integration of rainfall thresholds and susceptibility maps in the Emilia Romagna (Italy) regional-scale landslide warning system, Landslides, 12, 773-785, 2015.

Segoni, S., Rosi, A., Lagomarsino, D., Fanti, R., and Casagli, N.: Brief communication: Using averaged soil moisture estimates to improve the performances of a regional-scale landslide early warning system, Natural Hazards and Earth System Sciences, 18, 807-812, 2018.

Skamarock, W., Klemp, J., Dudhia, J., Gill, D., Barker, D., Duda, M., Huang, X., Wang, W., and Powers, J.: A description of the advanced research WRF Version 3, NCAR technical note, Mesoscale and Microscale Meteorology Division, National Center for Atmospheric Research, Boulder, Colorado, USA, 2008.

Hydrol. Earth Syst. Sci. Discuss., https://doi.org/10.5194/hess-2019-95
Manuscript under review for journal Hydrol. Earth Syst. Sci.
Discussion started: 22 March 2019



Skamarock, W. C., Klemp, J. B., Dudhia, J., Gill, D. O., Barker, D. M., Wang, W., and Powers, J. G.: A description of the advanced research WRF version 2, National Center For Atmospheric Research Boulder Co Mesoscale and Microscale Meteorology Div, 2005.

Srivastava, P. K., Han, D., Rico-Ramirez, M. A., Al-Shrafany, D., and Islam, T.: Data fusion techniques for improving soil moisture deficit using SMOS satellite and WRF-NOAH land surface model, Water resources management, 27, 5069-5087, 2013a.

Srivastava, P. K., Han, D., Rico Ramirez, M. A., and Islam, T.: Comparative assessment of evapotranspiration derived from NCEP and ECMWF global datasets through Weather Research and Forecasting model, Atmospheric Science Letters, 14, 118-125, 2013b.

Srivastava, P. K., Han, D., Rico-Ramirez, M. A., O'Neill, P., Islam, T., Gupta, M., and Dai, Q.: Performance evaluation of WRF-Noah Land surface model estimated soil moisture for hydrological application: Synergistic evaluation using SMOS retrieved soil moisture, Journal of Hydrology, 529, 200-212, 2015.

Stéfanon, M., Drobinski, P., D'Andrea, F., Lebeaupin-Brossier, C., and Bastin, S.: Soil moisture-temperature feedbacks at meso-scale during summer heat waves over Western Europe, Climate dynamics, 42, 1309-1324, 2014.

Temimi, M., Leconte, R., Chaouch, N., Sukumal, P., Khanbilvardi, R., and Brissette, F.: A combination of remote sensing data and topographic attributes for the spatial and temporal monitoring of soil wetness, Journal of Hydrology, 388, 28-40, 2010.

Thompson, G., Field, P. R., Rasmussen, R. M., and Hall, W. D.: Explicit forecasts of winter precipitation using an improved bulk microphysics scheme. Part II: Implementation of a new snow parameterization, Monthly Weather Review, 136, 5095-5115, 2008.

Tsai, T.-L., and Chen, H.-F.: Effects of degree of saturation on shallow landslides triggered by rainfall, Environmental Earth Sciences, 59, 1285-1295, 2010.

Valenzuela, P., Domínguez-Cuesta, M. J., García, M. A. M., and Jiménez-Sánchez, M.: Rainfall thresholds for the triggering of landslides considering previous soil moisture conditions (Asturias, NW Spain), Landslides, 15, 273-282, 2018.

Wei, J., Dirmeyer, P. A., Guo, Z., Zhang, L., and Misra, V.: How much do different land models matter for climate simulation? Part I: Climatology and variability, Journal of Climate, 23, 3120-3134, 2010.

Wharton, S., Simpson, M., Osuna, J., Newman, J., and Biraud, S.: Assessment of Land Surface Model Performance in WRF for Simulating Wind at Heights Relevant to the Wind Energy Community, Lawrence Livermore National Lab.(LLNL), Livermore, CA (United States), 2013.

Wilks, D.: Statistical Methods in the Atmospheric Sciences, 3rd ed., Academic Press, 2011.

Yang, Z. L., Niu, G. Y., Mitchell, K. E., Chen, F., Ek, M. B., Barlage, M., Longuevergne, L., Manning, K., Niyogi, D., and Tewari, M.: The community Noah land surface model with multiparameterization options (Noah-MP): 2. Evaluation over global river basins, Journal of Geophysical Research: Atmospheres, 116, 2011.

Zaidi, S. M., and Gisen, J. I. A.: Evaluation of Weather Research and Forecasting (WRF) Microphysics single moment class-3 and class-6 in Precipitation Forecast, MATEC Web of Conferences, 2018, 03007, Zaitchik, B. F., Santanello, J. A., Kumar, S. V., and Peters-Lidard, C. D.: Representation of soil moisture feedbacks during drought in NASA unified WRF (NU-WRF), Journal of Hydrometeorology, 14, 360-367, 2013.

Zeng, X., and Decker, M.: Improving the numerical solution of soil moisture–based Richards equation for land models with a deep or shallow water table, Journal of Hydrometeorology, 10, 308-319, 2009.

Zêzere, J. L., Trigo, R. M., and Trigo, I. F.: Shallow and deep landslides induced by rainfall in the Lisbon region (Portugal): assessment of relationships with the North Atlantic Oscillation, Natural Hazards and Earth System Science, 5, 331-344, 2005.

Zhuo, L., Dai, Q., and Han, D.: Evaluation of SMOS soil moisture retrievals over the central United States for hydro-meteorological application, Physics and Chemistry of the Earth, Parts A/B/C, 83, 146-155, 2015a.

Zhuo, L., Han, D., Dai, Q., Islam, T., and Srivastava, P. K.: Appraisal of NLDAS-2 multi-model simulated soil moistures for hydrological modelling, Water resources management, 29, 3503-3517, 2015b.

Zhuo, L., Dai, Q., Islam, T., and Han, D.: Error distribution modelling of satellite soil moisture measurements for hydrological applications, Hydrological Processes, 30, 2223-2236, 2016a.

Zhuo, L., and Han, D.: Misrepresentation and amendment of soil moisture in conceptual hydrological modelling, Journal of Hydrology, 535, 637-651, 2016a.

Zhuo, L., and Han, D.: Could operational hydrological models be made compatible with satellite soil moisture observations?, Hydrological Processes, 30, 1637-1648, 2016b.

Hydrol. Earth Syst. Sci. Discuss., https://doi.org/10.5194/hess-2019-95
Manuscript under review for journal Hydrol. Earth Syst. Sci.
Discussion started: 22 March 2019


Hydrology and Earth System Sciences
Discussions

Zhuo, L., Han, D., and Dai, Q.: Soil moisture deficit estimation using satellite multi-angle brightness temperature, Journal of Hydrology, 539, 392-405, 2016b.

Zhuo, L., Dai, Q., Han, D., Chen, N., Zhao, B., and Berti, M.: Evaluation of remotely sensed soil moisture for landslide hazard assessment, IEEE Journal of Selected Topics in Applied Earth Observations and Remote Sensing, 12, 162 - 173, 2019.

Hydrol. Earth Syst. Sci. Discuss., https://doi.org/10.5194/hess-2019-95
Manuscript under review for journal Hydrol. Earth Syst. Sci.
Discussion started: 22 March 2019




**Table 1.** Comparison of Noah, Noah-MP, and CLM4.

| | Noah | Noah-MP | CLM4 |
|---|---|---|---|
| Energy balance | Yes | Yes | Yes |
| Water balance | Yes | Yes | Yes |
| No. of soil layers | 4 | 4 | 10 |
| Depth of total soil column | 2.0 m | 2.0 m | 3.802 m |
| Model soil layer thickness | 0.1, 0.3, 0.6, 1.0 m | 0.1, 0.3, 0.6, 1.0 m | 0.018, 0.028, 0.045, 0.075, 0.124, 0.204, 0.336, 0.553, 0.913, 1.506 m |
| No. of vegetation layers | A single combined surface layer of vegetation and snow | Single layer | Single layer |
| Vegetation | Dominant vegetation type in one grid cell with prescribed LAI | Dominant vegetation type in one grid cell with dynamic LAI | Up to 10 vegetation types in one grid cell with prescribed LAI |
| No. of snow layers | A single combined surface layer of vegetation and snow | Up to three layers | Up to five layers |

Hydrol. Earth Syst. Sci. Discuss., https://doi.org/10.5194/hess-2019-95
Manuscript under review for journal Hydrol. Earth Syst. Sci.
Discussion started: 22 March 2019




**Table 2.** WRF parameterizations used in this study

| | Settings/ Parameterizations | References |
|---|---|---|
| Map projection | Lambert | |
| Central point of domain | Latitude: 44.54; Longitude: 11.02 | |
| Latitudinal grid length | 5 km | |
| Longitudinal grid length | 5 km | |
| Model output time step | Daily | |
| Nesting | Two-way | |
| Land surface model | Noah, Noah-MP, CLM | |
| Simulation period | 1/1/2006 – 31/12/2015 | |
| Spin-up period | 1/1/2005 – 31/12/2005 | |
| Microphysics | New Thompson | (Thompson et al., 2008) |
| Shortwave radiation | Dudhia scheme | (Dudhia, 1989) |
| Longwave radiation | Rapid Radiative Transfer Model | (Mlawer et al., 1997) |
| Surface layer | Revised MM5 | (Jiménez et al., 2012;Chen and Dudhia, 2001) |
| Planetary boundary layer | Yonsei University method | (Hong et al., 2006) |
| Cumulus Parameterization | Kain-Fritsch (new Eta) scheme | (Kain, 2004) |

Hydrol. Earth Syst. Sci. Discuss., https://doi.org/10.5194/hess-2019-95
Manuscript under review for journal Hydrol. Earth Syst. Sci.
Discussion started: 22 March 2019


Hydrology and Earth System Sciences
Open Access
Discussions

**Table 3.** Statistical summary of the WRF performance in simulating soil moisture for different soil layers, based on comparison with the in-situ observations.

| | R | | | | RMSE ($m^3/m^3$) | | | |
|---|---|---|---|---|---|---|---|---|
| | 0.10 m | 0.25 m | 0.70 m | 1.50 m | 0.1 m | 0.25 m | 0.70 m | 1.50 m |
| Noah | 0.728 | 0.645 | 0.660 | 0.430 | 0.123 | 0.125 | 0.141 | **0.055** |
| Noah-MP | **0.809** | 0.683 | **0.738** | **0.498** | **0.060** | **0.070** | **0.088** | 0.092 |
| CLM | 0.789 | **0.743** | 0.648 | 0.287 | 0.089 | 0.087 | 0.123 | 0.089 |

Hydrol. Earth Syst. Sci. Discuss., https://doi.org/10.5194/hess-2019-95
Manuscript under review for journal Hydrol. Earth Syst. Sci.
Discussion started: 22 March 2019




**Table 4.** Rainfall events information.

| Starting date | | | Ending date | | | Duration (days) | Rainfall intensity (mm/day) | Number of Landslide events |
|---|---|---|---|---|---|---|---|---|
| Year | Month | Day | Year | Month | Day | | | |
| 2014 | 1 | 13 | 2014 | 1 | 24 | 12 | 20.50 | 2 |
| 2014 | 1 | 28 | 2014 | 2 | 14 | 18 | 13.61 | 0 |
| 2014 | 2 | 26 | 2014 | 3 | 6 | 9 | 13.35 | 0 |
| 2014 | 3 | 22 | 2014 | 3 | 27 | 6 | 11.08 | 0 |
| 2014 | 4 | 4 | 2014 | 4 | 5 | 2 | 18.98 | 0 |
| 2014 | 4 | 27 | 2014 | 5 | 4 | 8 | 12.13 | 0 |
| 2014 | 5 | 26 | 2014 | 6 | 3 | 9 | 5.05 | 0 |
| 2014 | 6 | 14 | 2014 | 6 | 16 | 3 | 18.29 | 0 |
| 2014 | 6 | 25 | 2014 | 6 | 30 | 6 | 11.39 | 0 |
| 2014 | 7 | 7 | 2014 | 7 | 14 | 8 | 7.84 | 0 |
| 2014 | 7 | 21 | 2014 | 7 | 30 | 10 | 15.35 | 0 |
| 2014 | 8 | 31 | 2014 | 9 | 5 | 6 | 5.67 | 0 |
| 2014 | 9 | 10 | 2014 | 9 | 12 | 3 | 11.84 | 0 |
| 2014 | 9 | 19 | 2014 | 9 | 20 | 2 | 23.04 | 0 |
| 2014 | 10 | 1 | 2014 | 10 | 1 | 1 | 14.51 | 0 |
| 2014 | 10 | 10 | 2014 | 10 | 17 | 8 | 13.01 | 0 |
| 2014 | 11 | 4 | 2014 | 11 | 18 | 15 | 18.28 | 0 |
| 2014 | 11 | 25 | 2014 | 12 | 7 | 13 | 7.58 | 0 |
| 2014 | 12 | 13 | 2014 | 12 | 16 | 4 | 6.24 | 0 |
| 2015 | 1 | 16 | 2015 | 1 | 17 | 2 | 14.87 | 0 |
| 2015 | 1 | 21 | 2015 | 1 | 23 | 3 | 7.13 | 0 |
| 2015 | 1 | 29 | 2015 | 2 | 10 | 13 | 9.98 | 0 |
| 2015 | 2 | 13 | 2015 | 2 | 17 | 5 | 6.62 | 1 |
| 2015 | 2 | 21 | 2015 | 2 | 26 | 6 | 11.84 | 4 |
| 2015 | 3 | 3 | 2015 | 3 | 7 | 5 | 11.69 | 1 |
| 2015 | 3 | 15 | 2015 | 3 | 17 | 3 | 9.00 | 0 |
| 2015 | 3 | 21 | 2015 | 3 | 27 | 7 | 12.09 | 2 |
| 2015 | 4 | 3 | 2015 | 4 | 5 | 3 | 16.62 | 0 |
| 2015 | 4 | 17 | 2015 | 4 | 18 | 2 | 6.99 | 0 |
| 2015 | 4 | 26 | 2015 | 4 | 29 | 4 | 11.23 | 0 |
| 2015 | 5 | 15 | 2015 | 5 | 16 | 2 | 8.83 | 0 |
| 2015 | 5 | 20 | 2015 | 5 | 27 | 8 | 10.58 | 1 |
| 2015 | 6 | 8 | 2015 | 6 | 11 | 4 | 6.47 | 0 |
| 2015 | 6 | 16 | 2015 | 6 | 19 | 4 | 13.44 | 0 |
| 2015 | 6 | 23 | 2015 | 6 | 24 | 2 | 6.07 | 0 |
| 2015 | 7 | 22 | 2015 | 7 | 25 | 4 | 6.05 | 0 |
| 2015 | 8 | 9 | 2015 | 8 | 10 | 2 | 24.69 | 0 |
| 2015 | 8 | 15 | 2015 | 8 | 19 | 5 | 10.69 | 0 |
| 2015 | 8 | 23 | 2015 | 8 | 24 | 2 | 7.88 | 0 |
| 2015 | 9 | 13 | 2015 | 9 | 14 | 2 | 24.66 | 1 |
| 2015 | 9 | 23 | 2015 | 9 | 24 | 2 | 7.50 | 0 |
| 2015 | 10 | 1 | 2015 | 10 | 7 | 7 | 13.73 | 0 |
| 2015 | 10 | 10 | 2015 | 10 | 19 | 10 | 9.40 | 0 |
| 2015 | 10 | 27 | 2015 | 10 | 29 | 3 | 20.33 | 0 |
| 2015 | 11 | 21 | 2015 | 11 | 25 | 5 | 13.78 | 1 |

Hydrol. Earth Syst. Sci. Discuss., https://doi.org/10.5194/hess-2019-95
Manuscript under review for journal Hydrol. Earth Syst. Sci.
Discussion started: 22 March 2019


Hydrology and Earth System Sciences
Open Access
Discussions

**Table 5.** Results of Euclidean distances (*d*) between individual points and the optimal point for ROC analysis are listed. The best performance (i.e., lowest *d*) for each column (i.e., each soil layer of an LSM scheme) is highlighted. The optimal performance of all is highlighted in red.

| | Noah | | | | Noah-MP | | | | CLM4 | | | |
|---|---|---|---|---|---|---|---|---|---|---|---|---|
| *e.p. (%).* | 10 cm | 25 cm | 70 cm | 150 cm | 10 cm | 25 cm | 70 cm | 150 cm | 10 cm | 25 cm | 70 cm | 150 cm |
| 1 | 0.942 | 0.971 | 0.962 | 0.947 | 0.857 | 0.937 | 0.897 | 0.963 | 0.942 | 0.939 | 0.978 | 0.975 |
| 2 | 0.906 | 0.945 | 0.963 | 0.923 | 0.854 | 0.912 | 0.883 | 0.959 | 0.923 | 0.922 | 0.959 | 0.952 |
| 3 | 0.889 | 0.924 | 0.961 | 0.915 | 0.849 | 0.855 | 0.838 | 0.952 | 0.870 | 0.874 | 0.940 | 0.947 |
| 4 | 0.884 | 0.898 | 0.946 | 0.914 | 0.838 | 0.814 | 0.829 | 0.924 | 0.831 | 0.843 | 0.925 | 0.947 |
| 5 | 0.860 | 0.875 | 0.924 | 0.896 | 0.820 | 0.793 | 0.812 | 0.908 | 0.791 | 0.822 | 0.915 | 0.921 |
| 6 | 0.835 | 0.854 | 0.910 | 0.874 | 0.803 | 0.785 | 0.800 | 0.905 | 0.770 | 0.817 | 0.911 | 0.909 |
| 7 | 0.827 | 0.861 | 0.902 | 0.858 | 0.777 | 0.767 | 0.791 | 0.889 | 0.753 | 0.801 | 0.902 | 0.900 |
| 8 | 0.816 | 0.849 | 0.889 | 0.851 | 0.745 | 0.765 | 0.782 | 0.876 | 0.745 | 0.785 | 0.902 | 0.910 |
| 9 | 0.790 | 0.827 | 0.878 | 0.834 | 0.706 | 0.732 | 0.766 | 0.871 | 0.742 | 0.777 | 0.864 | 0.904 |
| 10 | 0.762 | 0.811 | 0.863 | 0.825 | 0.672 | 0.702 | 0.747 | 0.862 | 0.738 | 0.767 | 0.835 | 0.887 |
| 15 | 0.615 | 0.741 | 0.839 | 0.763 | 0.560 | 0.629 | 0.716 | 0.835 | 0.702 | 0.700 | 0.729 | 0.790 |
| 20 | 0.485 | 0.627 | 0.779 | 0.652 | 0.515 | 0.571 | 0.624 | 0.774 | 0.570 | 0.602 | 0.594 | 0.650 |
| 25 | 0.432 | 0.544 | 0.728 | 0.512 | 0.403 | 0.465 | 0.574 | 0.736 | 0.509 | 0.522 | 0.471 | 0.509 |
| 30 | 0.437 | 0.495 | 0.643 | 0.451 | **0.369** | **0.375** | 0.544 | 0.679 | 0.475 | 0.477 | 0.447 | 0.469 |
| 35 | **0.392** | 0.446 | 0.592 | 0.436 | 0.390 | 0.404 | 0.411 | 0.498 | 0.441 | 0.435 | 0.428 | 0.430 |
| 40 | 0.500 | **0.407** | 0.531 | 0.416 | 0.439 | 0.385 | **0.382** | 0.436 | **0.406** | **0.405** | **0.398** | **0.410** |
| 50 | 0.552 | 0.425 | **0.404** | **0.411** | 0.489 | 0.417 | 0.416 | **0.429** | 0.437 | 0.435 | 0.408 | 0.437 |

Hydrol. Earth Syst. Sci. Discuss., https://doi.org/10.5194/hess-2019-95
Manuscript under review for journal Hydrol. Earth Syst. Sci.
Discussion started: 22 March 2019

Hydrology and Earth System Sciences
Open Access
Discussions

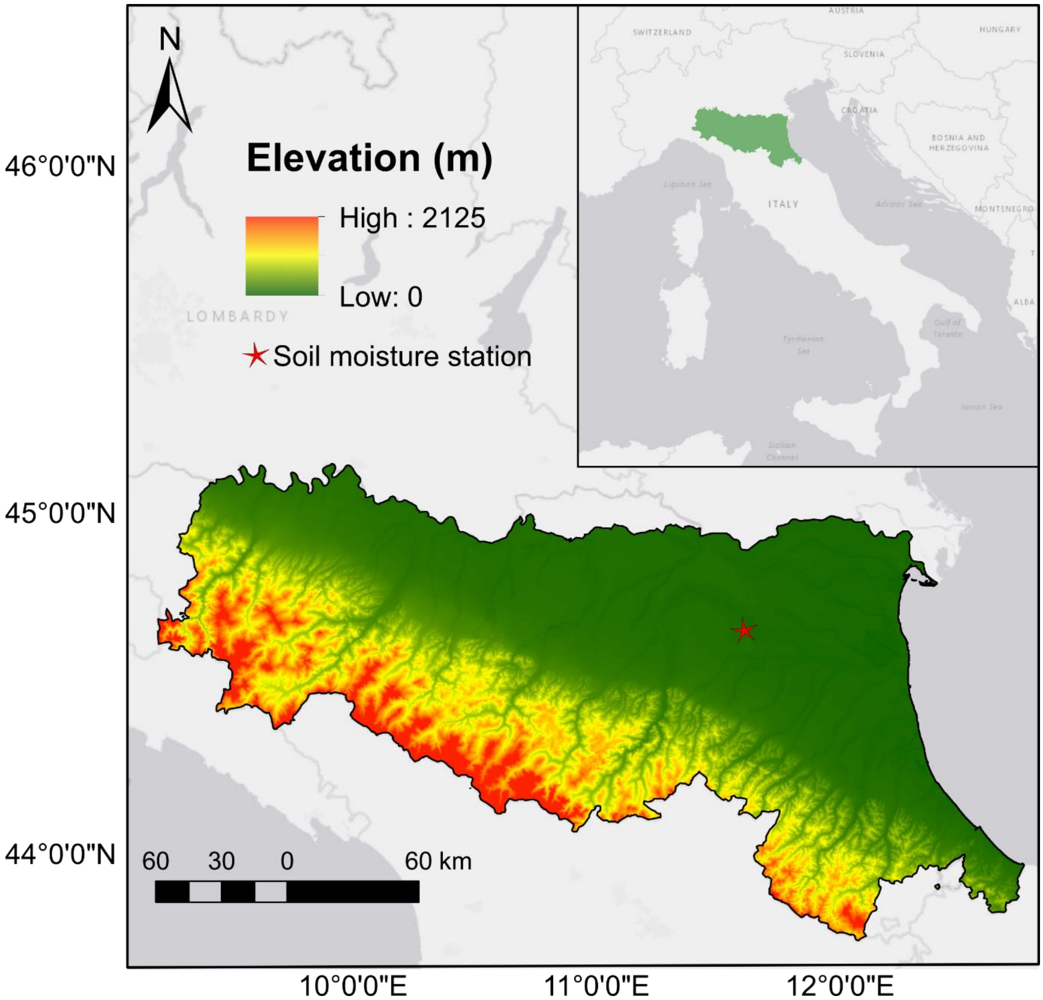


**Figure 1.** Location of the Emilia Romagna Region with elevation map and in-situ soil moisture station also shown.

Hydrology and Earth System Sciences
Open Access
Discussions

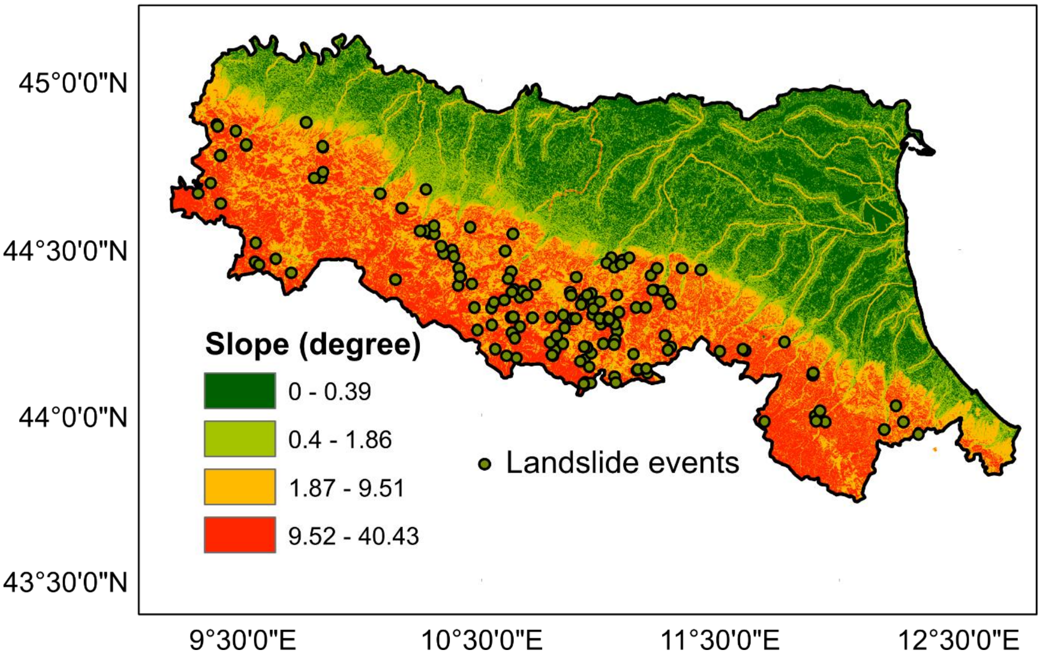


**Figure 2.** Landslide events with slope angle map.

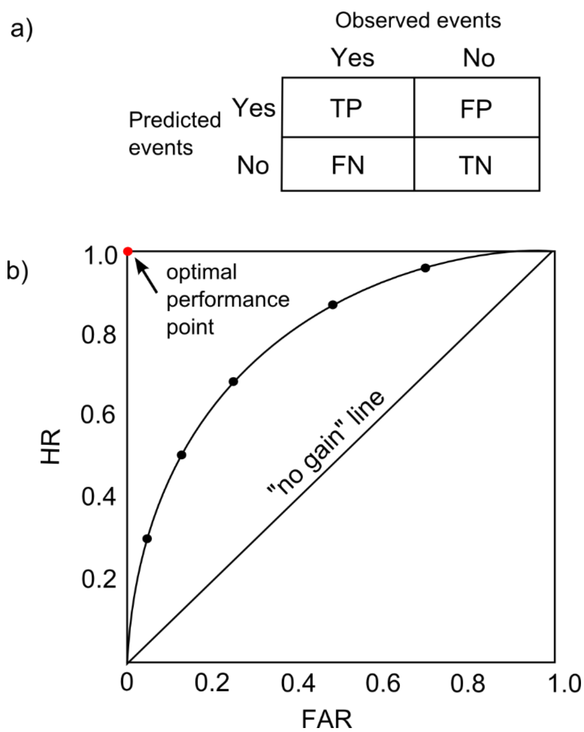


**Figure 3.** a) Contingency table illustrates the four possible outcomes of a binary classifier model: TP (True Positive), TN (True Negative), FP (False Positive), and FN (False Negative). b) ROC (Receiver Operating Characteristic) analysis with HR (Hitting Rate) against FAR (False Alarm Rate).

Hydrol. Earth Syst. Sci. Discuss., https://doi.org/10.5194/hess-2019-95
Manuscript under review for journal Hydrol. Earth Syst. Sci.
Discussion started: 22 March 2019


Hydrology and Earth System Sciences
Open Access
Discussions

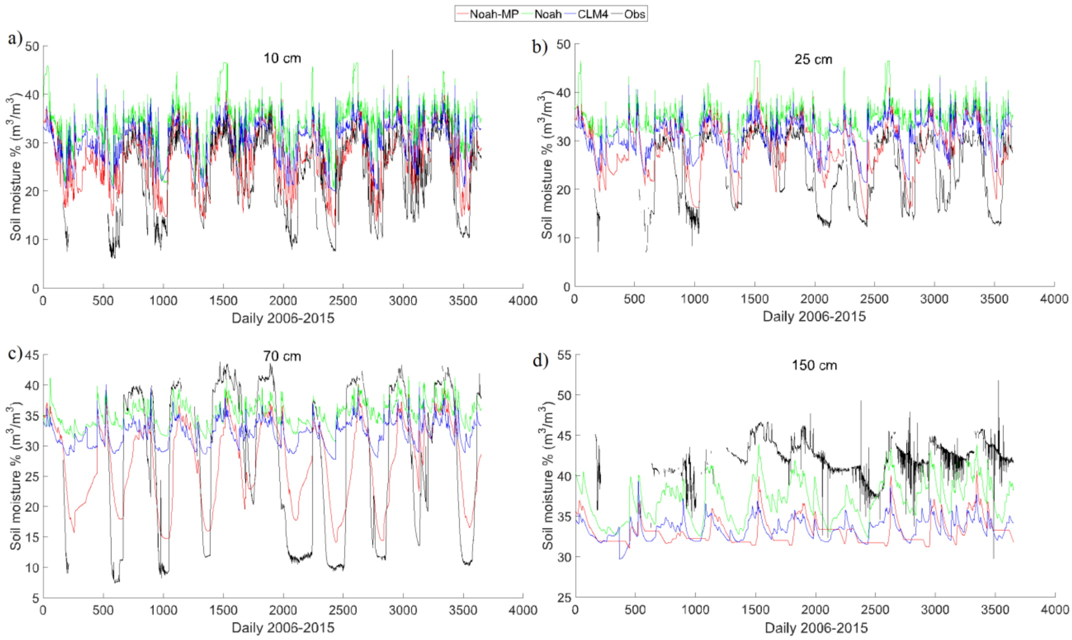


**Figure 4.** Soil moisture temporal variations of WRF simulations and in-situ observations for four soil layers at a) 10 cm; b) 25 cm; c) 70 cm; and d) 150 cm.

Hydrology and Earth System Sciences
Discussions

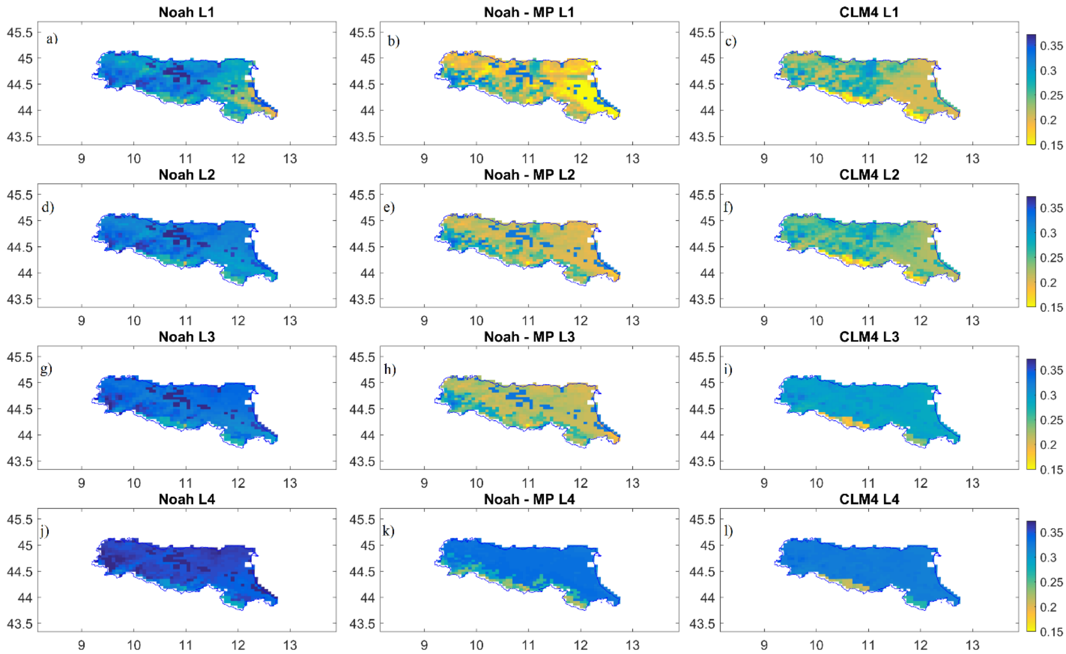


**Figure 5.** Spatial distribution of soil moisture at four soil layers (L1 = 10 cm; L2 = 25 cm; L3 = 70 cm; L4 = 150 cm) from WRF model simulations for Noah (a, d, g, j), Noah-MP (b, e, h, k), and CLM4 (c, f, i, l), on the August 1, 2015 (dry season).

Hydrol. Earth Syst. Sci. Discuss., https://doi.org/10.5194/hess-2019-95
Manuscript under review for journal Hydrol. Earth Syst. Sci.
Discussion started: 22 March 2019


Hydrology and Earth System Sciences
Discussions

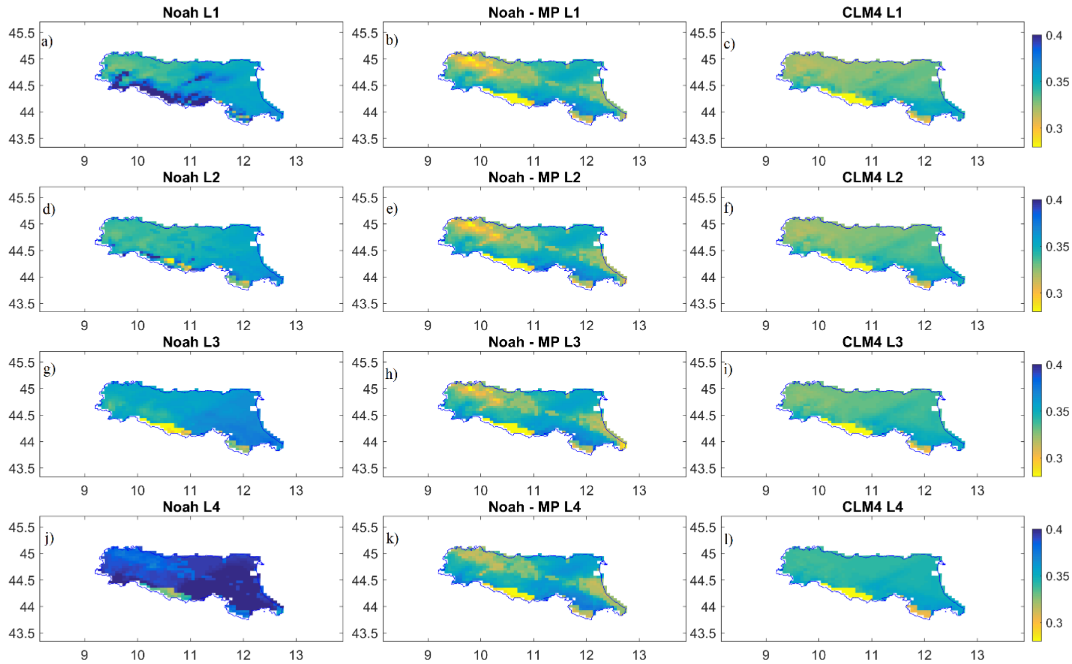


**Figure 6.** Spatial distribution of soil moisture at four soil layers (L1 = 10 cm; L2 = 25 cm; L3 = 70 cm; L4 = 150 cm) from WRF model simulations for Noah (a, d, g, j), Noah-MP (b, e, h, k), and CLM4 (c, f, i, l), on the February 1, 2015 (wet season).

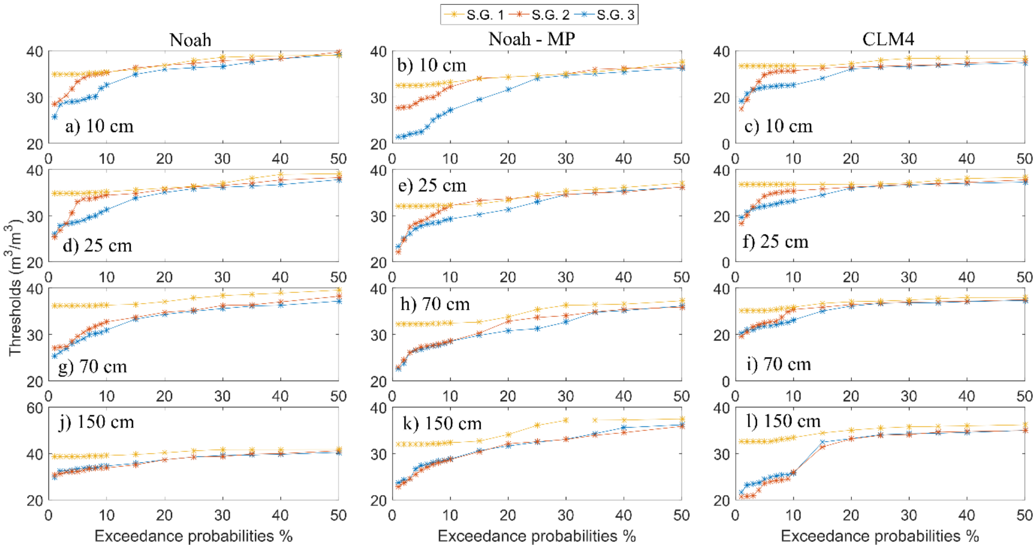


**Figure 7.** Threshold plots. For Noah (a, d, g, j), Noah-MP (b, e, h, k), and CLM4 (c, f, i, l) land surface schemes under three Slope angle Groups (S.G.) with S.G. 1 = 0.4-1.86°; S.G. 2 = 1.87-9.61°; S.G. 3 = 9.52-40.43°.

Hydrol. Earth Syst. Sci. Discuss., https://doi.org/10.5194/hess-2019-95
Manuscript under review for journal Hydrol. Earth Syst. Sci.
Discussion started: 22 March 2019


Hydrology and Earth System Sciences
Discussions

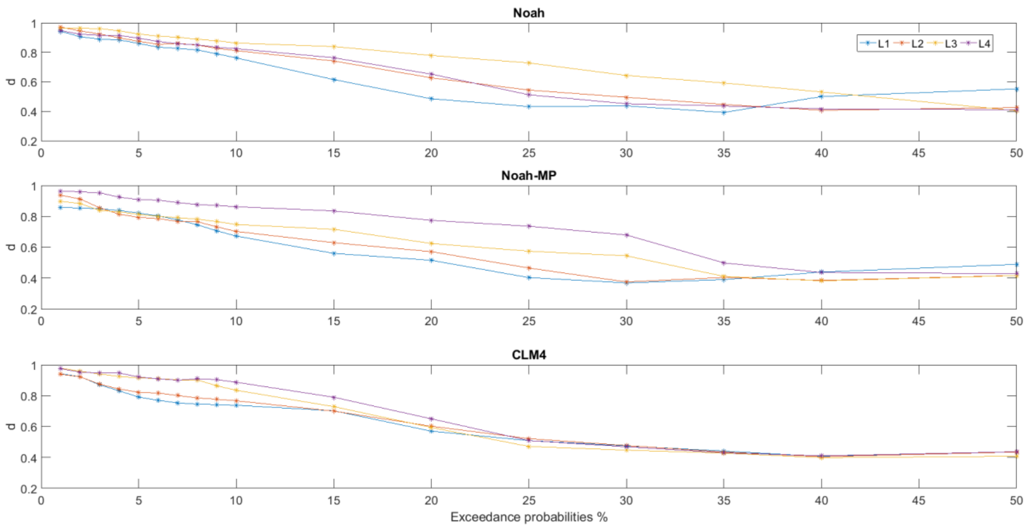


**Figure 8.** d-scores.

Hydrol. Earth Syst. Sci. Discuss., https://doi.org/10.5194/hess-2019-95
Manuscript under review for journal Hydrol. Earth Syst. Sci.
Discussion started: 22 March 2019


Hydrology and Earth System Sciences
Discussions

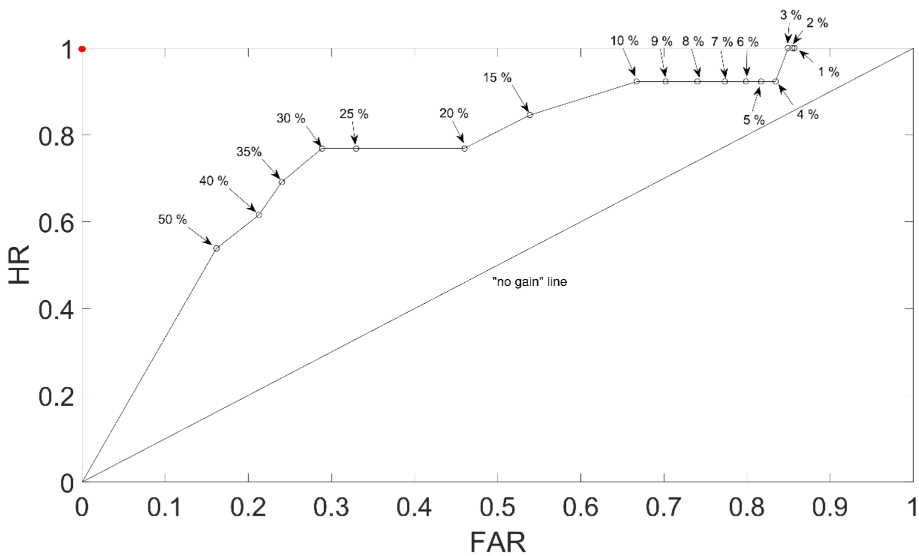


**Figure 9.** ROC curve for the calculated thresholds using different exceedance probability levels (for Noah-MP at the surface layer). The *no gain* line and the optimal performance point (the red point) are also presented.